Journal of Applied Electrochemistry (2007) 37:225–231
DOI 10.1007/s10800-006-9239-3

Chemical and morphological analyses of zinc powders for alkaline batteries

MARTIN G. PEREZ, MATTHEW J. O'KEEFE*, THOMAS O'KEEFE and DOUGLAS LUDLOW
Graduate Center for Materials Research, University of Missouri-Rolla, Rolla, MO, 65409, USA
*(*author for correspondence, tel.: + 1-573-341-6764, fax: + 1-573-341-2071, e-mail: mjokeefe@umr.edu)*

Received 27 February 2006; accepted in revised form 12 September 2006

Key words: alkaline batteries, hydrogen gassing, zinc oxide, zinc powders, zinc powder morphology, zinc powder surface chemistry

Abstract

Zinc powders containing Bi, In and either Mg or Al were analyzed to determine chemical and morphological differences. Morphology and chemistry may influence the reactivity of Zn powders in the basic environment found inside alkaline batteries. Increased reactivity leads to increased Zn corrosion, increased hydrogen gas evolution, and possibly leakage of the battery electrolyte. The surface chemistry of the powders was examined using Auger electron spectroscopy, X-ray photoelectron spectroscopy, and atomic absorption spectroscopy to check for surface ZnO. Powder chemistry was measured using an electron probe micro analyzer equipped with an energy dispersive X-ray analyzer. Inert gas fusion determined the bulk oxygen content. Morphology studies included powder sieving for size determination, examining loose powders with a scanning electron microscope (SEM), and determining surface areas via Brunauer, Emmet, and Teller (BET) analyses. SEM images showed differences in powder shapes and surface conditions between passed and failed powders. Powders exhibiting smooth surfaces and regular shapes were more likely to pass gas testing. However, pass/fail gas test results could not be correlated to powder chemistry, powder size, or surface area. Powder roughness and irregularity may indicate an increase in the number of active sites such as peaks and barbs versus particles with smooth surfaces.

1. Introduction

Zinc powders serve as the anode material in commercial alkaline batteries. The anode is a paste of alloyed Zn powder, 35–45% KOH solution and proprietary additives. While the battery is in storage, the Zn anode corrodes, and hydrogen gas and zincate ions are generated as byproducts [1–3]. With sufficient hydrogen gas build-up, the battery seals may rupture which will cause the electrolyte to leak out. Factors such as storage temperature, electrolyte chemistry, powder composition and powder morphology influence the gassing behavior of the Zn anode [1, 2].

Previously, Hg was alloyed with Zn to slow down the corrosion process [4, 5]. A Hg-containing phase was identified on the surface of Zn powders (1.5–7% Hg by weight) that increased the hydrogen overpotential of the anode by ~100 mV and reduced hydrogen gassing [4]. The increased hydrogen overpotential provided less cathodic current to drive the corrosion process. Other methods of modifying the Zn powders surface included the use of organic inhibitors [6–8], the addition of Pb [2], the addition of indium hydroxide to plate In over the Zn metal by a displacement reaction [6], or adding In_2O_3 [9].

Strict environmental and health regulations have outlawed the use of Hg and Pb in alkaline batteries [1, 2]. Bismuth and In have been substituted for Hg and Pb, because they also increased the hydrogen overpotential of the Zn anode [9–11]. Their concentrations in commercial Zn alloy powders are typically < 1000 ppm. Bismuth and In have an extremely low solubility in Zn, and no known Zn–Bi, Zn–In or Zn–Bi–In phase has been reported [12–14]. The Bi and In segregate, and they can be expected to form three Bi–In phases: BiIn, Bi_3In_5, and $BiIn_2$ [15].

Trace additions of metals that readily form oxides, such as Al, may also be added to commercial Zn powders to act as surface deoxidizers [16]. Aluminum may smooth out Zn powder surfaces. Miura et al. predicted that Al enhanced the high temperature oxidation resistance of Zn during atomization. Oxidation increases microscopic surface roughness and acts against liquid surface tension. Increased liquid surface tension promotes smooth surfaces in powders. The addition of Al produced smaller powder sizes relative to pure Zn powders produced under the same conditions. This powder refinement was also observed for Zn–Ni powders. Upon solidification, a smooth, regularly shaped powder may result. Miura et al. also reported that Al

inhibits Zn corrosion within a specific range of concentrations. Zn powders with 0.1 wt.% Al inhibited corrosion while 1.0 wt.% Al promoted corrosion.

A ZnO layer may also influence the hydrogen evolution properties of the Zn anode [7, 9, 11]. Ogai et al. reported that a three fold increase in the ZnO content increased the hydrogen gassing levels by three to four times [11]. Sato et al. postulated that if Zn comes in contact with solid ZnO, some of the electrons generated by the oxidation of Zn into $Zn(OH)^{2-}$ may instead reduce some of the ZnO already present on the powder surface [9]. The result is very active Zn which is the same formed by electrolysis. The Zn will immediately react with H_2O to reform ZnO and evolve hydrogen gas.

The role of Mg is not clear, but it may act as grain refiner or deoxidizer. The addition of Mg or Al in Zn castings increases the fluidity or viscosity of the melts [17]. The fluidity may affect the Zn liquid surface tension, possibly affecting powder size and surface condition [18].

In this study, commercial grade, air atomized Zn powders containing three alloy elements, Bi, In and either Al or Mg were obtained and analyzed to correlate the surface chemistry, surface ZnO content, bulk chemistry, and morphology to hydrogen gas testing results. Total alloy concentrations were <1000 ppm. Powders that had gassing levels below the manufacturer's gas specification limit (passed) were directly compared to powders that had gas levels above the manufacturer's specification limit (failed). Morphological attributes such as surface condition, size and shape were examined for effects on the surface area since a high surface area may increase the reactivity of the powders [19, 20].

2. Experimental procedure

To attain representative Zn powder distributions, all tests and analyses used powders that were mixed in a Turbula mixer for 10 min [18, 21]. Two types of commercial Zn powders were examined: Zn–Bi–In–Al (BIA powders) and Zn–Bi–In–Mg (BIM powders). To compare the size distributions of the different powders, approximately 50 g of each powder type was sieved for 15 min in a Fritch Laborgeratebau shaking table.

Two methodologies were implemented to measure surface chemistry. X-ray photoelectron spectroscopy (XPS) with Mg K_α radiation and Auger electron spectroscopy (AES) were used to measure the amounts of Bi, In, O, Mg or Al near the powder surfaces. Loose powders were mounted on a specimen holder with an adhesive surface. Zinc powders were analyzed using a Kratos Analytical Axis 165 X-ray photoelectron spectrometer (XPS) and a Physical Electronics Model 545 Auger electron spectrometer (AES). All XPS samples were Ar sputter etched for 120 s. Data was collected from an area 600 μm by 800 μm in size. Sputter time for the AES was 30 min at a rate of 1.5 nm per minute, to a depth of 45 nm. As a supplemental analysis, the surface ZnO content was measured using a Varian SpectrAA 50 atomic absorption spectrometer (AA). The ZnO was dissolved in a 5% aqueous ammonia solution.

The bulk chemistry of the powders was checked for alloy concentrations and oxygen levels. The chemical composition of the powders was determined using an electron probe micro analyzer (EPMA) equipped with an energy dispersive X-ray analyzer (EDXA). Phases present in the microstructure were analyzed with an electron beam of spot size of 200 nm in diameter. Inert gas fusion tests determined the bulk oxygen content of 2–3 g of Zn powder. The samples were melted in a graphite crucible inside an induction furnace under vacuum and held at 2000 °C [22, 23].

Polished powder microstructures and loose powders shapes and surfaces were examined with a Hitachi S570 scanning electron microscopes (SEM) or with a Hitachi S4700 Field Emission SEM (FESEM). Both SEMs were equipped with an energy dispersive X-ray spectrometer (EDS). Powder morphologies were classified based on a criteria established by German [19]. Krypton BET measurements were done on a Quantachrome Autosorb Automated Gas Sorption System. Either 14 or 20 g of Zn powders were degassed under vacuum at 250 °C for 48–72 h prior to taking BET measurements. The BET results were accepted if the correlation coefficient was >0.99 [18, 24, 25]. As a complement to the study, the surfaces of specially made high concentration powders were inspected under the SEM for the presence of alloying elements. These high concentration powders were manufactured in a pilot plant air atomizer at the manufacturer's site, and they had concentrations that were 20 times higher than those of commercial powders. The powders were especially made for electron backscatter diffraction analyses (EBSD) from a different study.

3. Results and discussion

3.1. *Powder microstructural analysis*

Backscatter electron images (BSE) for virgin BIA and BIM powders showed that the microstructure consisted of Zn and a type of Bi–In phase (i.e., BiIn, Bi_3In_5, or $BiIn_2$), which segregated to the Zn grain boundaries (Figure 1(a)). The SEM images showed the Bi–In phases to be <300 nm in size and located 5–15 μm below the powder surfaces (Figure 1(b)). Polished powder cross sections and loose powders were checked for the presence a Bi–In phase or a continuous layer that may be indicative of surface ZnO. Only Zn was detected.

Powders with high Bi and In concentrations contained a high density of Bi–In particles that were >1 μm in size (Figure 2). The Bi–In phases on the surfaces of production powders were difficult to locate in the SEM due to their small diameters ($\ll 300$ nm) and low particle

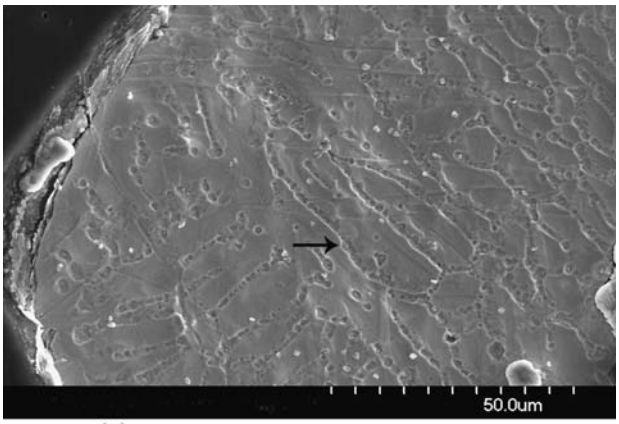

(a) Microstructure of single powder (BSE 1000X).

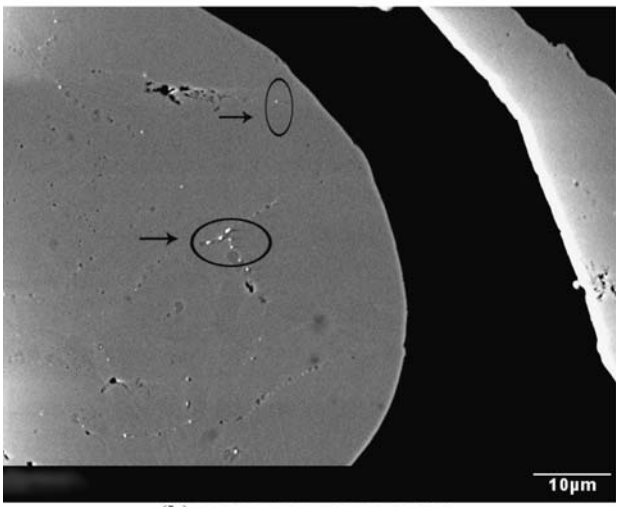

(b) BIM-F1 (BSE 1300X) – Failed

Fig. 1. (a) Zn powder microstructure. Arrow points to location in grain boundary where Bi and In are located. (b) BIM powder microstructure with Bi–In phases located 5–15 μm below the surface of a Zn powder. No ZnO was observed at the powder edge or surface.

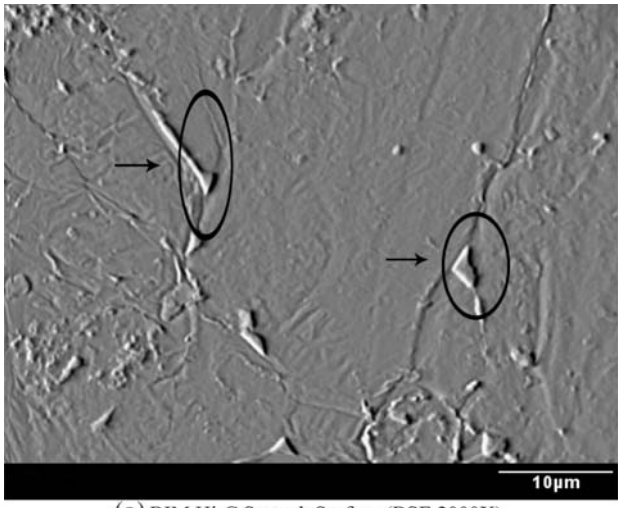

(a) BIM Hi-C Smooth Surface (BSE 2000X)

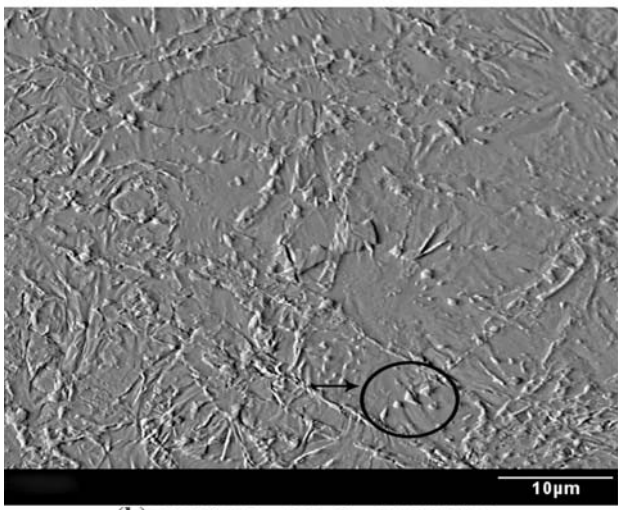

(b) BIM Hi-C Rough Surface (BSE 2000X)

Fig. 2. BSE images of BIM high concentration, loose powder surfaces. Arrows point to location of Bi-In phases. (a) BIM Hi-C Smooth Surface (BSE 2000×). (b) BIM Hi-C Rough Surface (BSE 2000×).

density. The discovery of Bi–In phases on the powder surfaces of the high Bi–In containing phases indicated that Bi and In might also be found on the surfaces of commercial Zn powders and that the powders may not have a continuous layer of pure Zn as shown in the polished cross sections. Surface chemical analyses were required to correlate the Bi and In concentrations to hydrogen gassing performance.

The surfaces of powders that had undergone gas testing were also examined for the presence of surface ZnO. Polished cross sections of BIM powders had Zn grain boundaries extending to the surface but no visible ZnO layer. If a very thin ZnO layer was present on the Zn surfaces, it may have been a few nanometers thick and not visible in the SEM.

3.2. *Surface chemical analysis*

X-ray photoelectron spectroscopy detected equivalent concentrations of O, Bi, or In content between BIM Zn powder surfaces (Table 1). XPS was unable to detect Mg in the BIM powders because the binding energies corresponding to Mg overlap with those of Zn. AES was then used to determine the Mg concentrations. AES data showed no significant differences in the amount of Bi, In, O, or Mg in the BIM Zn alloy powders. Expanded AES depth profiles for Bi and In contents between passed and failed powders are shown in Figure 3.

Table 1. XPS results for Zn powders after sputter etching[a]

Powder	Atomic concentration % (± 0.1 at. %)						
	Zn	C	O	Bi	In	Mg	Al
BIM-F1	19.0	38.6	41.5	0.3	0.6	Not detected	–
BIM-P1	17.0	45.1	36.8	0.3	0.8	Not detected	–
BIM-F2	20.9	39.1	39.6	0.2	0.2	Not detected	–
BIA-F1	10.8	47.0	33.6	0.2	0.3	–	8.1
BIA-P1	17.2	39.6	39.5	0.2	0.1	–	3.5

[a]F designation = failed powder per manufacturer's gas tests. P = passed.

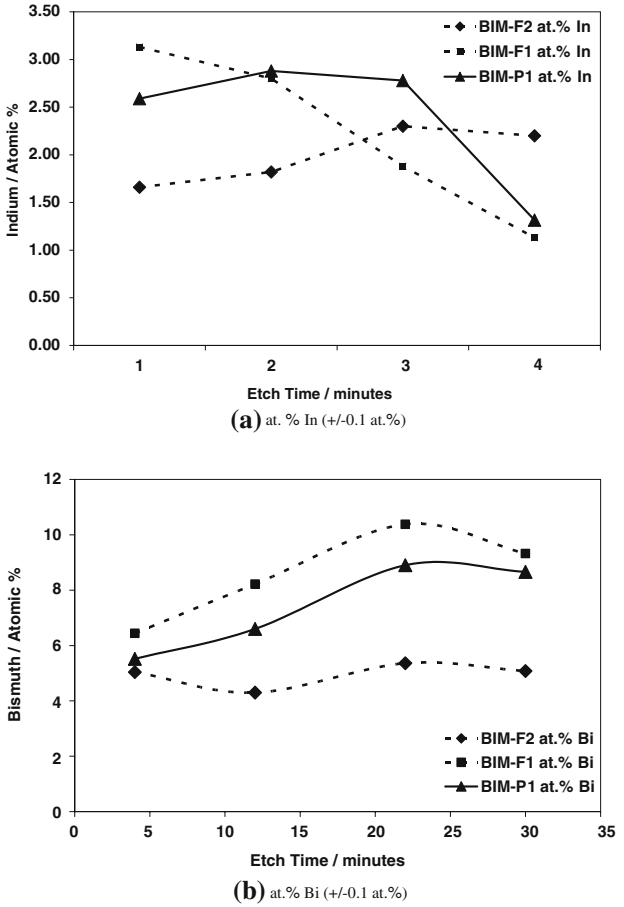

Fig. 3. Expanded AES profiles for Bi and In in BIM powders. Averages are shown. Dotted lines are for powders that failed gas testing.

X-ray photoelectron spectroscopy detected a higher Al content in a failed BIA powder versus one that passed (Table 1). After 120 s of Ar sputter etching, the passed BIA-P1 powder gave a reading of 3.5 at.% Al (3.9 wt.%) versus 8.1at.% Al (10.5 wt.%) for BIA-F1. The relative differences in Al suggest that a higher Al content may contribute to a higher gassing behavior. Equivalent amounts of O, Bi, and In were detected for both powders by XPS. The ZnO contents were similar

Table 2. Two sample *t*-test results: Bi/In wt.% ratios for Zn powders ($\alpha = 0.05$)[a]

Comparison	Avg. Bi/In wt.% ratio (±SD)	*p*-value from 2-sample *t*-test	Statistical difference between means?
BIM-F1 vs. BIM-P1	1.2 ± 0.1 1.2 ± 0.2	0.88	No
BIM-P1 vs. BIM-F2	1.2 ± 0.2 1.5 ± 0.4	0.029	Yes
BIM-F1 vs. BIM-F2	1.2 ± 0.1 1.5 ± 0.4	0.019	Yes
BIA-F1 vs. BIA-P1	1.0 ± 0.5 0.9 ± 0.2	0.75	No

[a]F designation = failed powder per manufacturer's gas tests.
P = passed.

Table 3. Inert gas fusion tests for bulk oxygen content of Zn alloy powders[a]

Powder	Oxygen concentration/ppm
BIM-F1	140
BIM-P1	200
BIM-F2	160
BIA-F1	240
BIA-P1	220

[a]F designation = failed powder per manufacturer's gas tests.
P = passed.

for the four BIA powders tested by AA, as 0.13–0.17 wt.% of ZnO was detected for all the powders.

3.3. *Bulk chemical analysis*

The bulk chemistry was also checked for alloy content and oxygen concentrations. The Bi and In data from the

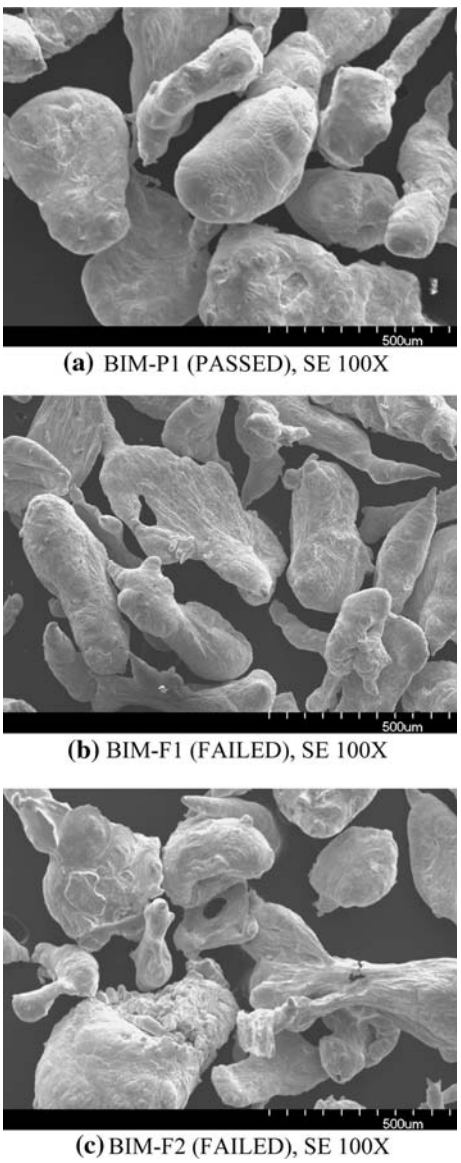

Fig. 4. SEM images of BIM virgin loose powders. (a) BIM-P1 (passed), SE 100×. (b) BIM-F1 (failed), SE 100×. (c) BIM-F2 (failed), SE 100×.

Table 4. Qualitative analysis of surface conditions and morphology of BIA Zn alloy powders[a]

Powder	Surface type	Morphology type	Gas test prediction	Actual gas test result
BIA-P4	Rough	II & III	Fail	X – Pass
BIA-P5	Rough	I & IV	Fail	X – Pass
BIA-F4	Rough larges, smooth smalls	II & III	Fail	Fail
BIA-F5	Rough larges, smooth smalls	I & II	Fail	Fail
BIA-F6	Rough larges, smooth smalls	I & II	Pass	X – Fail
BIA-F7	Mix rough & smooth	IV	Fail	Fail
BIA-P6	Mix rough & smooth	I & III	Pass	Pass
BIA-P7	Smooth	I	Pass	Pass
BIA-P8	Smooth	I & III	Pass	Pass
BIA-P9	Smooth	I & III	Pass	Pass

Morphology Types: I – Round, regular, small; II – Large, regular shape; III – Elongated; IV – Irregular [a]F designation = failed powder per manufacturer's gas tests. P = passed.

EPMA were used to calculate Bi/In wt.% ratios. The Zn data was ignored in calculating the Bi/In wt.% ratios. Aluminum and Mg were not detected. A two sample *t*-test ($\alpha = 0.05$) was run using Minitab statistical software to detect differences in the bulk Bi and In compositions (Table 2). The average Bi/In wt.% ratio was the response variable, and a *p*-value $< \alpha$ indicated that there was a statistical difference in the mean Bi/In wt.% ratios [26]. The Bi/In wt.% ratios for the powders ranged between 0.9 and 1.5, but the statistical differences between these values were not significant enough to conclude that real differences exist between powder chemistries. The average Bi/In wt.% ratios between passed and failed BIM and BIA powders were statistically equivalent. One of the failed BIM powders had a higher Bi/In wt.% ratio, but this may be attributed to sampling error. The BIM and BIA powders also had very similar bulk oxygen concentrations in the range of 140–200 ppm (Table 3). No trend was found between oxygen concentrations and gassing.

3.4. *Powder morphology*

Noticeable differences were observed between the morphologies of passed and failed BIM powders. Images of passed BIM-P1 powders showed that the shapes were rounded or ligamental and had relatively smooth surfaces (Figure 4(a)). In contrast, BIM-F1 and BIM-F2 failed powders exhibited irregular shapes, relatively rougher surfaces and had satellites (Figure 4(b) and (c)).

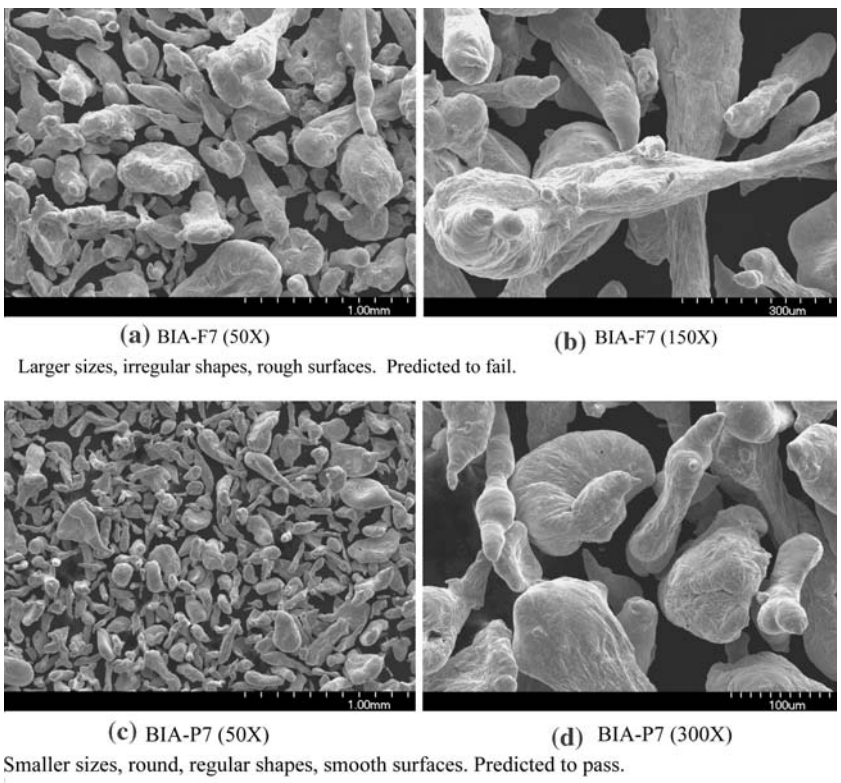

Fig. 5. Qualitative comparison of two BIA powders for shape, size and surface roughness. (a) BIA-F7 (50×), (b) BIA-F7 (150×) (Larger sizes, irregular shapes, rough surfaces. Predicted to fail). (c) BIA-P7 (50×), (d) BIA-P7 (300×) (Smaller sizes, round, regular shapes, smooth surfaces. Predicted to pass).

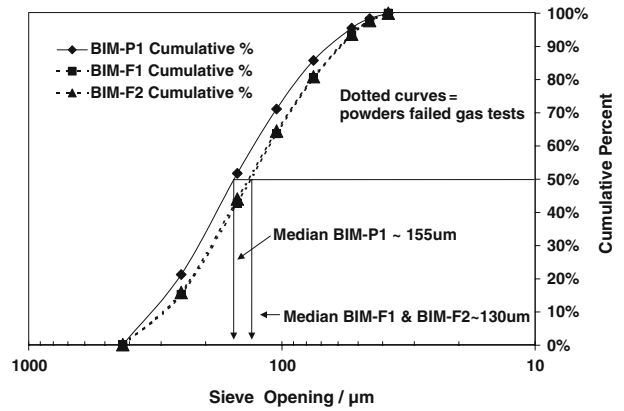

(a) Cumulative Percent of BIM Powders

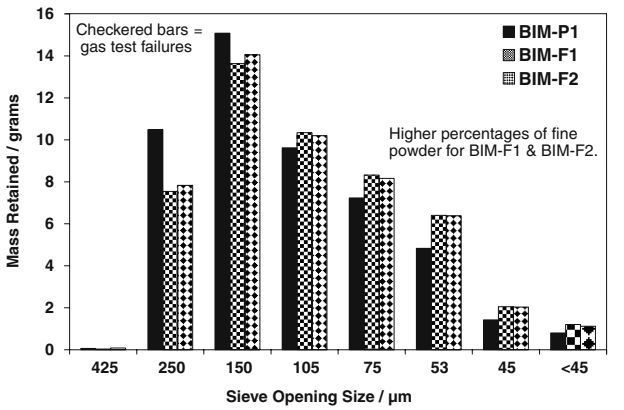

(b) Histogram for BIM Powders

Fig. 6. Sieve data for BIM powders. (a) Cumulative percent of BIM powders. (b) Histogram for BIM powders.

These were considered as characteristics of higher chemical reactivity. A qualitative test, based on the observed BIM powder morphologies, was used to predict a pass/fail gas test result for the BIA powders.

The gas test predictions for the BIA powders based on morphology were 70% accurate when compared to the actual manufacturer test results (Table 4). The BIA powders were qualitatively rated for surface conditions and shape. A powder sample with smooth surface, rounded, regular shapes was likely to pass gas testing.

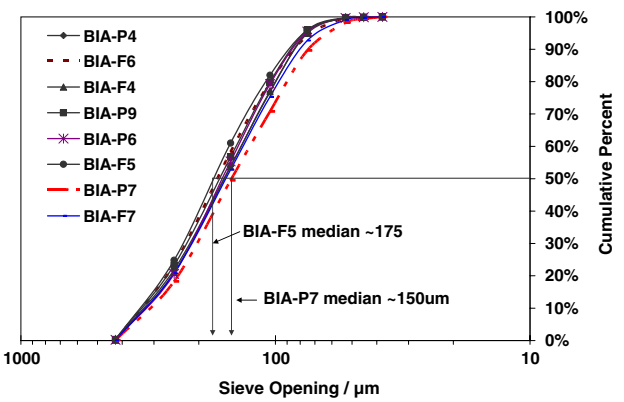

Fig. 7. BIA powders size distributions.

Conversely, a powder samples with an irregular shape may be expected to fail gas testing. Sample BIA-F7 had large particles, irregular shapes, relatively rough surfaces and was predicted to fail (Figure 5(a)). The BIA-P7 powder is an example of a powder showing small particles with rounded, regular shapes and relatively smooth surfaces and was expected to pass (Figure 5(c)). For powders showing a wide range of particle sizes and different surface conditions, predictions were based on the overall surface condition of the large particles. Large particles with relatively rougher surfaces were predicted to fail, but these powders actually passed the manufacturer's gas tests (BIA-P4, P5). Incorrect gas test predictions were attributed to errors in powder sampling.

The failed BIM powders had a higher percentage of fine and subsieve powders, which may have generated higher gassing due to an increased surface area. (dotted curves in Figure 6(a) and checkered bars in Figure 6(b)). The BIA powders appeared to be well matched for size (Figure 7). A gas test prediction based on powder size could not be made for the BIA powders.

The BIA powders had similar surface area values as measured by BET (Table 5). Krypton BET results revealed that the Zn powders had surface areas $< 1\ m^2$. The SEM images of Zn powder surfaces were observed to be dense and had a low surface porosity. This may have led to low specific surface areas. All BET tests were limited to ~20 g, the BET cell capacity. A greater quantity of Zn powder would provide for more total surface area and should increase the accuracy of the BET analysis.

4. Conclusions

For the BIM and BIA powders, increased hydrogen gas evolution may better be explained by differences in the observed powder morphology than differences in powder chemistry measurements. Surface and bulk chemical analyses of Zn powders were shown to have equivalent alloy additions and oxygen contents. The BIA powders may be an exception, with the failing powder having a higher Al concentration. Difficulties in accurately measuring differences in chemistry were attributed to total alloy concentrations of < 1000 ppm. The Bi and In alloying elements, which affect the hydrogen overpotential of the Zn anode, were less of a factor than originally envisioned for determining the high gassing rates of the failed powders. Microstructures showed the Bi-In phases segregating to the Zn grain boundaries. Since no trend was identified in the AA, this strongly suggested that equivalent amounts of surface ZnO was formed during the atomization process. The small differences in powder chemistry pointed to the physical attributes of the powder as being a stronger contributor to hydrogen gas evolution.

The observed powder morphology provided the basis for a qualitative test to make gas test pass/fail predictions. Powders with mainly rough surfaces or exhibiting

Table 5. Kr BET Results for BIA Powders[a]

BIA Powder	Surface type	Gas test prediction	Actual gas test result	Specific surface area, $\times 10^{-2}/m^2\ g^{-1}$
BIA-P4	Rough	Fail	X – Pass	2.5
BIA-P5	Rough	Fail	X – Pass	2.2
BIA-F4	Rough larges, smooth smalls	Fail	Fail	2.9
BIA-F5	Rough larges, smooth smalls	Fail	Fail	2.7
BIA-F6	Rough larges, smooth smalls	Pass	X - Fail	2.9
BIA-F7	Mix rough & smooth	Fail	Fail	3.0
BIA-P6	Mix rough & smooth	Pass	Pass	2.7
BIA-P7	Smooth	Pass	Pass	2.9
BIA-P8	Smooth	Pass	Pass	2.9
BIA-P9	Smooth	Pass	Pass	2.4

All correlation coefficients are >0.99. Error: $\pm 0.01\ m^2\ g^{-1} \times 10^{-2}$.
[a]F designation = failed powder per manufacturer's gas tests. P = passed.

irregular shapes were predicted to fail gas testing, because they contained active sites in the form of satellites, barbs, spikes, and ridges. These sites may be considered as localized, high surface areas, and their formation may be attributed to variables in the atomization process. The BIA powders that underwent the qualitative morphology test had equivalent surface areas as measured by Kr BET. The low surface porosity on the Zn powders and the available sample sizes for BET measurements did not provide enough surface area to detect possible differences. Finally, the correlation between powder size and gassing was inconsistent. Hydrogen gas evolution may be exacerbated if a powder population contained noticeably higher amounts of fines or sub-sieve powders as measured in BIM powders.

Acknowledgements

Support for Martin Perez was provided by a fellowship through the National Science Foundation Integrative Graduate Education and Research Traineeship Program (DGE-9972752). Special thanks are extended to Dr. Yoshi Kato for the Japanese translation of the article in Denki Kagaku.

References

1. X.G. Zhang, *Corrosion and Electrochemistry of Zinc* (Plenum Press, New York, 1996) 373 pp.
2. L.O. Binder, in J.O. Besenhard (ed.), 'Handbook of Battery Materials', (Wiley-VCH, New York, 1999) pp. 200–206.
3. D.M. Jones, *Principles and Prevention of Corrosion* (MacMillan, New York, 1992) 5 pp.
4. M. Meeus, Y. Strauven and L. Groothaert, New developments in the production of mercury content in zinc powder for alkaline dry batteries, Power Sources: Proceedings of the 15th International Power Sources Symposium, Brighton, England, 22–25 September (1986) pp. 281–299.
5. T.S. Lee, *J. Electrochem. Soc.* **122** (1975) 171.
6. H. Yoshizawa and A. Miura, *Prog. Batteries Battery Mater.* **12** (1993) 132.
7. M. Yano, S. Fujitani and K. Nishio, *J. Appl. Electrochem.* **28** (1998) 1221.
8. J.M. Wang, Y.D. Qian, J.Q. Zhang and C.N. Cao, *J. Appl. Electrochem.* **30** (2000) 113.
9. Y. Sato, M. Takhashi, H. Asakura, T. Yoshida, K. Tada and K. Kobayakawa, *J. Power Sources* **38** (1992) 317.
10. M. Yano, S. Fujitani, K. Nishio, Y. Akai and M. Kurimura, *J. Power Sources* **74** (1998) 129.
11. K. Ogai, E. Mieno and J. Nakagawa (1995) Zinc alloy powder for alkaline batteries, Zinc & Lead '95, An International Symposium on the Extraction and Application of Zinc and Lead, Sendai, Japan, 22–24 May (1995) pp. 898–907.
12. M. Hansen, *Constitution of Binary Alloys* (McGraw-Hill, New York, 1958) 347 pp.
13. F.A. Shunk, Constitution of Binary Alloys, Second Supplement (McGraw-Hill, New York, 1969) 138 pp.
14. I.A. Lapkina, O.V. Sorokina and V.B. Ufimtsev, *Russ. J. Inorg. Chem.* **28** (1983) 1490.
15. H. Okamoto, *in* T.B. Massalski (ed.), 'Binary Alloy Phase Diagrams' Vol. 1, (American Society for Metals, Materials Park, OH, 1986) pp.748–751.
16. A. Miura, K. Takata, R. Okazaki, H. Ogawa, T. Uemura, Y. Nakamura and N. Kasahara, *Denki Kagaku oyobi Kogyo Busturi Kagaku* **57** (1989) 459.
17. D.C.H. Nevision, *in* D.M. Stefanescu, J.R. Davis, J.D. Destefani and T.B. Zorc 'ASM Handbook: Casting', Vol. 15, (ASM International, Materials Park, OH, 1998) pp.788.
18. R.M. German, *Powder Metallurgy Science* (Metal Powders Industry Federation, Princeton, NJ, 1994) 28 pp.
19. F. Habashi, Kinetics of Metallurgical Processes (Metallurgie Extractive Quebec, Sainte-Foy, Quebec, 1999) 106 pp.
20. G. Dube, R. Renaud and J.Y. Huot, *Prog. Batteries Battery Mater.* **10** (1991) 151.
21. Metal Powder Industries Federation. Standard Test Methods for Metal Powders and Powder Metallurgy Products, 1993–1994 ed., (Princeton, NJ, 1993).
22. Shivatec Home Page, http://www.shivatec.com, (accessed Nov 2004).
23. R.B. Fricioni and L. Essig, *in* R.E. Whan, K. Mills, J.R. Davis, J.D. Stefani, D.A. Dieterich, G.M. Crankovic and H.J. Frissell (eds) 'ASM Handbook: Materials Characterization', Vol. 10, (ASM International, Materials Park, OH, 1996) pp. 226–232.
24. S. Lowell and J.E. Shields, Powder Surface Area and Porosity (Chapman Hall, New York, 1991) 7 pp.
25. F.V. Lenel, *in* E. Klar (ed.) 'ASM Handbook: Powder Metallurgy', Vol. 7, (ASM International, Materials Park, OH, 1993) pp. 262–263.
26. D.C. Montgomery, Design and Analysis of Experiments (John Wiley & Sons, New York, 2001) 21 pp.